https://doi.org/10.5194/acp-2019-811
Preprint. Discussion started: 19 November 2019

Atmospheric Chemistry and Physics Discussions

Uptake selectivity of Methanesulfonic Acid (MSA) on fine particles over polynya regions of the Ross Sea, Antarctica

Jinpei Yan[*1,2], Jinyoung Jung[3], Miming Zhang[1,2], Federico Bianchi[4], Yee Jun Tham[4], Suqing Xu[1,2], Qi Lin[1,2], Shuhui Zhao[1,2], Lei Li[5], Liqi Chen[1,2]

1 Key Laboratory of Global Change and Marine-Atmospheric Chemistry, Xiamen 361005, China;
2 Third Institute of Oceanography, Ministry of Natural Resources, Xiamen 361005, China;
3 Korea Polar Research Institute, 26 Songdomirae-ro, Yeonsu-gu, Incheon 21990, Republic of Korea;
4 Institute for Atmospheric and Earth System Research; University of Helsinki, 00014, Finland;
5 Institute of Mass Spectrometer and Atmospheric Environment, Jinan University, Guangzhou 510632, China

Abstract: The uptake of methanesulfonic acid (MSA) on existing particles is a major route of the particulate MSA formation, however, MSA uptake on different particles is still lack of knowledge. Characteristics of MSA uptake on different aerosol particles were investigated in polynya regions of the Ross Sea, Antarctica. Particulate MSA mass concentrations, as well as aerosol populations and size distributions, were observed simultaneously for the first time to access the uptake of MSA on different particles. The results showed that MSA mass concentration did not always reflect MSA particle population in the marine atmosphere. MSA uptake on aerosol particles increased the particle size and changed aerosol chemical compositions, but did not increase the particle population. The uptake rates of MSA on existing particles were significantly influenced by aerosol chemical properties. The favor uptake of MSA occurred on the sea salt particles, as MSA-Na and MSA-Mg particles were abundant in the Na and Mg particles, accounting for 0.43±0.21 and 0.41±0.20 of the total Na and Mg particles, respectively. However, acidic and hydrophobic particles suppressed the MSA uptake, as MSA-EC and MSA-SO_4^{2-} accounted only 0.24±0.68 and 0.26±0.47 of the total EC and SO_4^{2-} particles, respectively. The results extended the knowledge of the formation and environmental behavior of MSA in the marine atmosphere.

Keywords: Methanesulfonic acid (MSA); nss-SO_4^{2-}; aerosol; climate change; Antarctica

1. Introduction

*Corresponding author. Tel.: +86 592 2195370; Fax: +86 592 2195280, E-mail address: jpyan@tio.org.cn; Address: No.178 Daxue Road, Siming district Xiamen, Third Institute of Oceanography, MNR, 361005, P R China.

https://doi.org/10.5194/acp-2019-811
Preprint. Discussion started: 19 November 2019

Atmospheric Chemistry and Physics Discussions

Methanesulfonic acid (MSA) and non-sea-salt-sulfate (nss-SO_4^{2-}), deriving from the oxidation of dimethyl sulfide (DMS), are important sources of cloud condensation nuclei (CCN) in the marine boundary layer (Chang et al., 2011; Ghahremaninezhad et al., 2016). Different from nss-SO_4^{2-}, MSA is exclusively from the oxidation of DMS in the atmosphere (Sorooshian et al., 2007). Thus, MSA was expected as a useful marker for the deconvolution of sulfate from marine biogenic and non biogenic sources (Legrand et al., 1998).The ratio of MSA to nss-SO_4^{2-} is often used to assess the DMS oxidation routes and the contributions of biogenic sulfur to other sulfur sources (Sorooshian et al., 2007; Wang et al., 2014). DMS oxidation routes, as well as the products of MSA and nss-SO_4^{2-}, have been investigated previously in the marine atmosphere (Preunkert et al., 2008; Kloster et al., 2006).

Generally, particulate MSA was generated from the reactive uptake of DMS and condensation of gaseous MSA on aerosol particles (Davis et al., 1998; Barnes et al., 2006). A recent study showed that MSA may increase sulfate cluster formation rate by up to one order of magnitude, increasing the stability of the clusters (Bork et al., 2014). However, previous studies have showed that SO_4^{2-} was more effective at new particle formation (NPF) than MSA, while MSA was more likely to condense onto existing particles (Hayashida et al., 2017). Although the reactive uptake of MSA on fine particles was demonstrated in the previous studies (Sorooshian et al., 2007; Bates et al., 1992), the influence of aerosol characteristics on MSA uptake has not been presented.

The chemical components and sources of aerosol particles in the marine atmosphere were rather complicated (Weller et al., 2018). Filtered sample methods were often used in previous studies (Jung et al., 2014; Preunkert et al., 2007; Read et al., 2008) with a long sampling interval to accommodate the detection limit of the instrument (Preunkert et al., 2007; Zhang et al., 2015). It is, therefore, difficult to clarify how MSA mixes with other aerosol species, using bulk aerosol sampling methods, as only the mean aerosol chemical components were presented during the sampling period (Bates et al., 1992; Chen et al., 2012). On-line aerosol mass spectrometry has been used to characterize the aerosol chemical species and sizes with high-time-resolution (Yan et al., 2018; Healy et al., 2010), allowing the determination of particle mixing states and sources. Although a few studies have shown that MSA was often associated with Mg in aerosol particles, probably due to marine biogenic activity (Casillas-Ituarte et al., 2010), studies of the interactions

https://doi.org/10.5194/acp-2019-811
Preprint. Discussion started: 19 November 2019

Atmospheric Chemistry and Physics Discussions

between MSA and other aerosol species were rare. Theoretical and laboratory studies have attempted to explain these observations and determine in which state MSA enters the aerosol particles (Bork et al., 2014). However，the relative likelihood of MSA uptake on different particles remains uncertain.

In this study, we examined the uptake characteristics of MSA on different particles over polynya regions in the Ross Sea (RS), Antarctica, based on high-time-resolution observations. MSA mass concentrations and particle populations, as well as aerosol compositions and size distributions, were measured simultaneously for the first time in the RS using an in-situ gas and aerosol compositions (IGAC) and a single particle aerosol mass spectrometer (SPAMS) monitoring instruments. Observations were carried out in two different seasons, the early December with intensity sea ice coverage and in the mid-January to February with sea ice free in the RS. The selectivity of MSA uptake on different particles was investigated in the RS with different circumstances.

2. Experiment methods and observation regions

The observations were carried out on-board of R/V "Xuelong", covering a large region of the RS, Antarctica (50°S to 78°S, 160°E to 185°E) (Fig. S1) with different sea ice concentrations. The leg I was carried out from December 2 to 20, 2017. The sea surfaces were covered with intense sea ices in the RS during this period (Fig. S4a). However, when we arrived back in the RS (leg II, from January 13 to February 14, 2018), the sea ices have almost melted in the RS (Fig. S4b).

2.1 Observation instruments and sampling inlet

An in-situ gas and aerosol compositions monitoring system (IGAC, Model S-611, Machine Shop, Fortelice International Co., Ltd., Taiwan; http://www.machine-shop.com.tw/), and a single particle aerosol mass spectrometer (SPAMS, Hexin Analysis Instrument Co., Ltd.) were used to determine aerosol water-soluble ion species, particle size distributions and chemical compositions,

https://doi.org/10.5194/acp-2019-811
Preprint. Discussion started: 19 November 2019

Atmospheric Chemistry and Physics Discussions

78 respectively (Fig. S2). The sampling inlet connecting to the monitoring instruments was fixed to a
79 mast 20 meters above the sea surface. A total suspended particulate (TSP) sampling inlet was
80 positioned at the top of the mast. Conductive silicon tubing with an inner diameter of 1.0 cm was
81 used to make the connection to all instruments.

82 **2.2 Aerosol water-soluble ion species**

83 Gases and aerosol water-soluble ion species were determined using a semi-continuous IGAC
84 monitor. Gases and aerosols were separated and streamed into a liquid effluent for on-line
85 chemical analysis at an hourly temporal resolution (Young et al., 2016; Liu et al., 2017). The
86 analytical design and methodology for the determination of gases and aerosol water-soluble ions
87 have been described in detail by Tao (2018) and Tian (2017). Fine particles were firstly enlarged
88 by vapor condensation and subsequently accelerated through a conical-shaped impaction nozzle
89 and collected on the impaction plate. The samples were then subsequently analyzed for anions and
90 cations by an on-line ion chromatography (IC) system (DionexICS-3000). The injection loop size
91 was 500 μL for both anions and cations. Six to eight concentrations of standard solutions were
92 selected for calibration, depending on the target concentration, in which the R^2 was above 0.997
93 (Fig. S3). The detection limits for MSA^-, SO_4^{2-}, Na^+, and Cl^- were 0.09, 0.12, 0.03, and 0.03 μg/L
94 (aqueous solution), respectively.

95 **2.3 Aerosol size distribution and chemical compositions**

96 The detection method for fine particles using a SPAMS has been described in detail by Li (Li et
97 al., 2011; Li et al., 2014). Particles were introduced into the vacuum system through a critical
98 orifice, then focused and accelerated to form a particle beam with specific velocity. The particle
99 beam was passed through two continuous diode Nd: YAG lasers (532 nm), where the scattered
100 light was detected by two Photomultiplier Tubes (PMTs). The velocity of a single particle was

https://doi.org/10.5194/acp-2019-811
Preprint. Discussion started: 19 November 2019

Atmospheric Chemistry and Physics Discussions

then determined and converted into its aerodynamic diameter. The individual particle was ionized with a 266 nm Nd: YAG laser to produce positive and negative ions. The fragment ions were analyzed using a bipolar time-of-flight mass spectrometer. The power density of the ionization laser was kept at $1.56x10^8$ w/cm^2.

The particle size data and mass spectra were analyzed using the YAADA software toolkit (http://www.yaada.org/) (Allen 2005). An adaptive resonance theory based neural network algorithm (ART-2a) was applied to cluster individual particles into separate groups based on the presence and intensity of ion peaks in the single particle mass spectrum (Song et al., 1999), with a vigilance factor of 0.65, a learning rate of 0.05, and a maximum of 20 iterations.

2.4 Metrological data

Meteorological parameters such as temperature, humidity, wind speed, and direction were measured continuously using an automated meteorological station deployed in the R/V "Xuelong", which was located on the top deck of the vessel.

2.5 Satellite data of sea ice and chlorophyll-a

In this study, we used remote sensing data to show the spatial and temporal distribution of chlorophyll and sea ice concentrations in the study region. Due to the cloud effect and swath limits, we chose the 8-day datasets for the remote sensing of chlorophyll-a from MODIS-Aqua (http://oceancolor.gsfc.nasa.gov) with a spatial resolution of 4 km. We used the sea ice on centration data from the daily 3.125-km AMSR2 dataset (Spreen et al., 2008) (available at https://seaice.uni-bremen.de). Each grid of the gridded datasets with a sea ice concentration less than or equal to 15 % was regarded as comprising all water (Cavalieri et al., 2003). The time series of the total regional mean value in the study region was then plotted.

3. Results and discussion

3.1. Spatial distributions of MSA mass concentration and particle population

MSA mass concentrations and their populations were measured continuously in the RS. MSA concentrations ranged from 14.6 to 210.8 ng.m^{-3}, with an average of 43.8±22.1 ng.m^{-3} during leg

https://doi.org/10.5194/acp-2019-811
Preprint. Discussion started: 19 November 2019

Atmospheric Chemistry and Physics Discussions

I (Fig.1a), consisting with summertime MSA levels recorded at Halley station, averaging 35.3 ng.m^{-3} (75°39'S) and Dumont d'Urville station (66°40'S) (Minikin et al., 1998), averaging 49 ng.m^{-3}, but lower than those reported at Palmer station, averaging 122 ng.m^{-3} (64°77' S) (Savoie et al., 1993). The highest MSA levels occurred at the region (64° - 67° S), with an maximum value of 210.8 ng.m^{-3} (Fig. 1a), consisting with the previous observation results from the Southern Ocean (60 - 70° S; maximum MSA level of 260 ng.m^{-3}) (Chen et al., 2012). In this study, elevated MSA levels were associated with the dynamic sea ice edge at ~64° S, once the sea ice started to melt in the early December (Fig. S4a and Fig. S4c). The release of iron (De Baar et al., 1995; Wang et al., 2014) and algae (Lizotte et al., 2001; Loose et al., 2011) from sea ice increased phytoplankton numbers (Taylor et al., 2013), resulting in the increase of DMS generation and emission (Hayashida et al., 2017). This, in turn, increased MSA levels due to the oxidation of DMS in the atmosphere.

MSA particle populations (0.1 - 2.5 μm) were determined simultaneously by SPAMS during the leg I (Fig. 1b). The highest average hourly MSA particle population (507 ± 189) occurred at MP1 (68° - 72°S, 172°E) near the Antarctic continent, following by MP2 (65° - 68°S, 160° - 170° E), with an average particle population of 344 ± 334. High MSA particle populations were associated with high wind speeds in these regions (MP1 8.06 ± 1.86m/s; MP2 15.76 ± 3.93m/s; Fig. 2).

The MSA concentration ranged from 11.4 - 165.4 ng•m^{-3} (with an average of 38.8 ± 27.5 ng•m^{-3}) during leg II, and the MSA particle population ranged from 3 - 1666 (with an average of 168 ± 172; Fig. 1c and 1d). Extremely high MSA levels, with an average of 100.3 ± 18.6 ng•m^{-3}, were observed in the MA region (170.2° - 177.4°E, 68.2° - 77.8°S), but we did not observed high MSA

https://doi.org/10.5194/acp-2019-811
Preprint. Discussion started: 19 November 2019

Atmospheric Chemistry and Physics Discussions

particle populations in this region (with an average of 171 ± 159). High MSA particle numbers with low MSA concentrations occurred at MP1 and MP2 (Fig.1a and 1b). It indicated that MSA mass concentrations did not always reflect the MSA particle populations in the marine atmosphere. Generally, the uptake of MSA on aerosol surfaces (Read et al., 2008) only changed the aerosol size and chemical compositions, without varying their population. Hence, the MSA particle population was mainly associated with the aerosol number in the atmosphere, as more particles were provided for the uptake of MSA in high particle population. Though high levels of MSA would also increase the MSA population, high MSA mass concentrations with low MSA populations were observed in this study. This phenomenon occurred when low existing particle populations and high MSA mass concentrations were presented in the marine atmosphere.

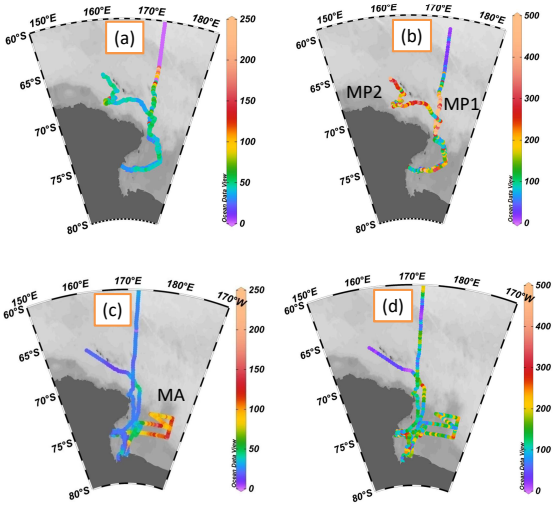

Fig.1 Spatial distribution of MSA mass concentrations and particle populations, (a) MSA mass concentrations during leg I (ng.m^{-3}); (b) MSA particle populations during leg I; (c) MSA mass concentrations during leg II (ng.m^{-3}) and (d) MSA particle populations during leg II.

3.2. Linkage between MSA concentration and particle population

To verify the relationship between MSA mass concentration and particle population, the temporal distributions of MSA mass concentration and particle number are illustrated in Fig. 2. Variations of MSA mass concentration were not always associated with the MSA particle

https://doi.org/10.5194/acp-2019-811
Preprint. Discussion started: 19 November 2019

Atmospheric Chemistry and Physics Discussions

167 population during the observation periods (Fig. 2a and Fig. 2b). MSA particle number did not
168 show an obvious correlation with MSA mass concentration (Fig. S5a), indicating that the major
169 factors regulating MSA mass concentration and MSA particle population were different. High
170 MSA particle populations often occurred in conjunction with high wind speeds (Fig. 2b and 2d),
171 while high MSA mass concentrations were not always observed at high wind speed regions, such
172 as extremely high MSA mass concentrations with low wind speeds were presented at MA (Fig. 2a,
173 2b and 2d).

174 MSA mass concentrations were determined by the oxidation of DMS, derived from marine
175 phytoplankton activity (Davis et al., 1998; Barnes et al., 2006; Read et al., 2008), but MSA
176 particle populations were mainly associated with the uptake of MSA on existing particles. High
177 existing particle populations led to high MSA particle populations, as the formation of particulate
178 MSA often occurred on the surfaces of existing particles (Read et al., 2008). In this study, the
179 variation of MSA particle population consisted with the variation of total particle population
180 during the observation period (Fig. 2b). A strong positive correlation between MSA particle
181 population and total particle population were presented (slope=0.19, r^2=0.65, n=1195, Fig. S5b).
182 The ratio of MSA particle population to total particle population ($R_{MSA/total}$) concentrated on the
183 range of 0.2 - 0.5, with an average of 0.29 ± 0.15 (Fig. 2b).

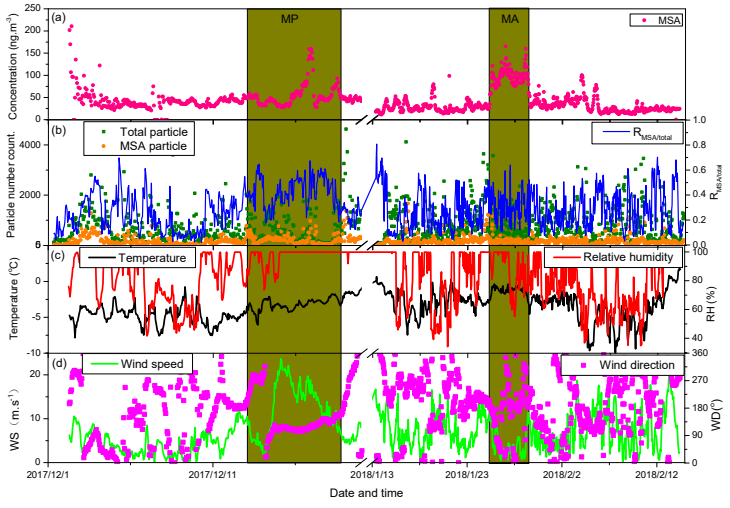

184

185 Fig. 2 Relationship between MSA mass concentration and MSA particle population in the context
186 of various environmental factors. (a) Time series of MSA mass concentrations; (b) Time series of

https://doi.org/10.5194/acp-2019-811
Preprint. Discussion started: 19 November 2019

Atmospheric Chemistry and Physics Discussions

MSA particle population, total particle population and the ratio of MSA particle population and total particle population; (c) Time series of temperature and relative humidity and (d) Time series of wind speeds and direction.

3.3. Signatures of MSA particle types

During leg I, 332438 single particles with positive and negative mass spectra were obtained, while 603098 single particles with positive and negative mass spectra were obtained during leg II. MSA particles, identified during the cruise using the ART-2a algorithm (Song et al., 1999), accounted for 27.69 % and 22.08 % of the total particles during leg I and leg II, respectively. To investigate the interactions between MSA and other species, MSA particles were further classified into seven sub-types, including MSA-Na, MSA-Mg, MSA-SO_4^{2-}, MSA-K, MSA-EC, MSA-OC, and MSA-NO_x^-.

3.3.1 MSA-Na particles

Sodium, which is often associated with sea salt particles in the marine atmosphere (Teinila et al., 2014), is an important component of atmospheric aerosols in ocean regions (Yan et al., 2018). Fig. 3a illustrates the average mass spectra of MSA-Na particles during leg I and leg II. Strong Na^+ peaks with weak K^+, Ca^+, and Na_2Cl^+ peaks were observed in the positive spectrum, while strong $NaCl_2^-$ and MSA^- peaks with low Cl^-, HSO_4^-, NO_3^-, and O^- peaks were observed in the negative spectrum. Similar average mass spectra for MSA-Na particles were observed during leg I and leg II, even though the two measurements were carried out under different circumstances. MSA-Na particles were the most dominant type of MSA particles, accounting for more than 30 % of total MSA particles (Fig. 4).

3.3.2 MSA-Mg particles

Mg is another common component in ocean-derived particles, hence, such particles are often classified as sea salt particles in the marine atmosphere. However, some previous studies have

https://doi.org/10.5194/acp-2019-811
Preprint. Discussion started: 19 November 2019

Atmospheric Chemistry and Physics Discussions

shown that the chemical properties of Mg particles observed in marine environment were distinct from those of sea salt particles (Gaston et al., 2011). In this study, the mass spectral characteristics of MSA-Mg type particles included strong MSA^- and Mg peaks (Fig. 3b). In sea salt particles, the dominant peak was typically Na^+ rather than Mg^+ (Fig. 3a) due to the higher concentration of Na^+ in seawater (Guazzotti et al., 2001). Similar with MSA-Na type particles, strong Na^+ and $NaCl_2^-$ peaks with weak Cl^-, NO_3^-, K^+, and Ca^+ peaks were observed in the mass spectra, indicating that MSA-Mg type particles were also derived from sea salt particles. Strong positive correlation (r^2=0.95) between MSA-Na and MSA-Mg was presented in this study (Fig. S6), indicating that these two types of particles were derived from the same sources. However, the abundance of Mg^+ fragment ion relative to Na^+ fragment ion in MSA-Mg type particles was different from MSA-Na type particles, indicating that MSA-Mg particles were also affected by other sources. Studies have shown that Mg particles were correlated strongly with atmospheric DMS (r^2=0.76) (Gaston et al., 2011), indicating that Mg particles were also impacted by marine biological materials, such as cell debris or fragments, viruses, bacteria, or the organics released by lysed cells (Casillas-Ituarte et al., 2010; Gaston et al., 2011). Hence, MSA-Mg type particles were associated with both sea salt particles and biological emissions.

3.3.3 MSA-SO_4^{2-} particles

SO_4^{2-} may be derived from different sources, such as sea salt aerosols, anthropogenic emissions, marine biogenic and volcanic sources (Legrand et al., 1998). Strong signals, peeking at m/z -97 HSO_4^- and m/z -95 MSA^-, were presented in the negative spectrum (seen in Fig. 3c), consisting with previous studies with intense signals of HSO_4^- and MSA^-occurred at m/z -97 and m/z -95 (Gaston et al., 2011; Silva et al., 2000). The simultaneous present of K^+, Na^+, Al^+, and Fe^+

https://doi.org/10.5194/acp-2019-811
Preprint. Discussion started: 19 November 2019

Atmospheric Chemistry and Physics Discussions

peaks in the positive mass spectrum and $NaCl_2^-$, NO_3^-, C_4H^- and $C_2H_2^-$ peaks in the negative mass spectrum, suggesting that MSA-SO_4^{2-} particles were associated with different sources. This can be further demonstrated by the size distribution of MSA-SO_4^{2-} particles (Fig. 5), as MSA-SO_4^{2-} particles are found in both fine and coarse particles.

3.3.4 MSA-K particles

The positive mass spectrum of the MSA-K particles was dominated by a strong K^+ peak with weak Na^+, $C_2H_3^+$ and $C_3H_7^+$ peaks (Fig. 3d). Strong HSO_4^-, and MSA^- signals were presented in the negative mass spectrum. Abundance of organic ion fragments were observed in the mass spectra of MSA-K particles. Generally, K was expected as a marker of biomass-burning source in continental areas (Yan et al., 2018). However, the mass spectra of MSA-K particles observed here were very different from the mass spectra of K particles observed in continental areas, suggesting that K particles from marine sources were quite different from continental sources.

3.3.5 MSA-OC particles

OC particles are often associated with anthropogenic sources, such as vehicle and coal combustion (Silva et al., 2000; Stiaras et al., 2008), marine biogenic sources (Quinn et al., 2014) and secondary sources (e.g. photochemical reaction from their precursor organic gases) (Horne et al., 2018). The positive and negative mass spectra of MSA-OC were dominated by C_xH_y ion peaks (i.e., $C_2H_3^+$, C_3H^+, $C_3H_3^+$, $C_3H_4^+$, and $C_3H_7^+$; Fig. 3e). Strong signals of HSO_4^- and MSA^- fragment ions were also presented in the negative spectrum, while a few signals of Na^+ and Cl^- were observed in the positive mass spectrum (Fig. 3e).

3.3.6 MSA-EC particles

EC particles are often associated with primary emissions; that is, the incomplete combustion

https://doi.org/10.5194/acp-2019-811
Preprint. Discussion started: 19 November 2019

Atmospheric Chemistry and Physics Discussions

of carbon-containing materials (Murphy et al., 2009). In this study, MSA-EC particles were characterized by strong peaks of C_n^- (C_4^-, C_3^- and C_2^-) in the negative spectrum, while the positive mass spectrum were dominated by Ca^+ ions (Fig. 3f). Compare with the average mass spectra of MSA-OC particles, the abundances of MSA^- and HSO_4^- fragment ions were lower in MSA-EC particles, indicating that the uptake of MSA on EC particles might be more difficult than the uptake of MSA on OC particles. Similar with the mass spectra of MSA-OC particles, a few fragments of Na^+ and Cl^- were observed in the MSA-EC mass spectra, suggesting that MSA-OC and MSA-EC particles rarely mixed with sea salt particles.

3.3.7 MSA-NO_x^- particles

The negative spectrum of MSA-NO_x^- particle was dominated by strong peaks of MSA^-, NO_2^-, and NO_3^-, with weak $C_xH_y^-$, O^-, and Cl^- peaks (Fig. 3g). Strong Na^+, $(C_3H_3^+)/K^+$, and $(C_3H_4^+)/Ca^+$ peaks with weak Na_2Cl^+ and CaO^+ peaks were observed in the positive spectrum. Sea salt particles reacted with atmospheric HNO_3 easily to form nitrate and hydrogen chloride (Adachi et al., 2015). The abundance of Na^+, Cl^-, and $NaCl_2^-$ ions in the mass spectra of the MSA-NO_x^- particles demonstrated these particles were formed by the interaction between sea salt particles and NO_x^- in the marine atmosphere.

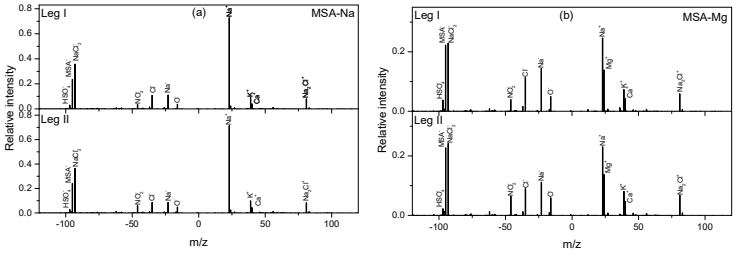

https://doi.org/10.5194/acp-2019-811
Preprint. Discussion started: 19 November 2019

Atmospheric Chemistry and Physics Discussions

272

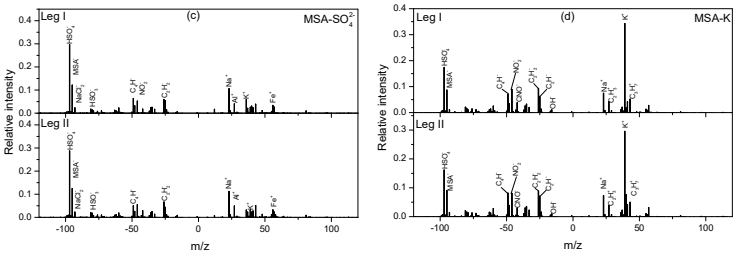

273

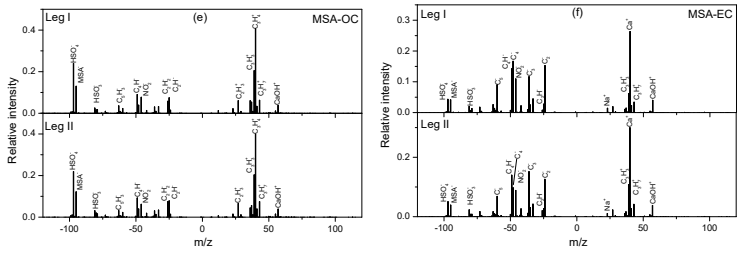

274

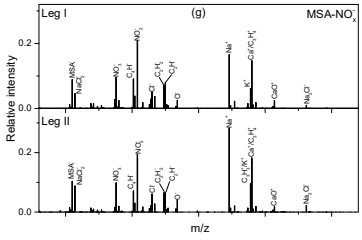

275 Fig. 3 Average mass spectra of major MSA clusters during leg I and leg II. (a) MAS-Na, (b)
276 MSA-Mg, (c) MSA-SO_4^{2-}, (d) MSA-K, (e) MSA-OC, (f) MSA-EC, and (g) MSA-NO_x^-.

277 **3.4 Uptake characteristics of MSA on existing particles**

278 In this study, Na, Mg, and SO_4^{2-} were the most abundant particles (Fig. 4a). Similar with Na,
279 Mg, and SO_4^{2-}, MSA-Na, MSA-Mg, and MSA-SO_4^{2-} were also the three most abundant MSA
280 particles (Fig. 4b), accounting for more than 70 % of the total MSA particles. It indicated that the
281 uptake of MSA was associated with the particle population. However, we found that SO_4^{2-} was the
282 most abundant particles of the total aerosol particles, while MSA-SO_4^{2-} was not the most abundant
283 MSA particles in the atmosphere. The results revealed that the formation of particulate MSA on
284 existing particles was affected by other factors, except particle population.

285 The average fractions of the MSA particle sub-types differed considerably from the average

https://doi.org/10.5194/acp-2019-811
Preprint. Discussion started: 19 November 2019

Atmospheric Chemistry and Physics Discussions

286 fractions of their corresponding particle types (Fig. 4c and 4d). SO_4^{2-} was the most abundant
287 particles, accounting for 26.8% of the total particles (Fig. 4c). However, MSA-SO_4^{2-} particles
288 accounted for only about 17.8% of the total MSA particles (Fig. 4d). Similarly, the relative
289 abundances of MSA-EC and MSA-K with respect to total MSA particles were lower than those of
290 EC and K with respect to the total particles. In contrast, MSA-Na particles were the most abundant
291 MSA particles, accounting for more than 32.55% of the total MSA particles (Fig. 4d), while Na
292 particles accounted for only 21.68% of the total particles (Fig. 4c). Similar patterns were observed
293 for Mg and OC particles. MSA-Mg and MSA-OC particles were more abundant in the MSA
294 particles than Mg and OC particles in the total particles (Fig. 4d). These results indicated that the
295 uptake of MSA on Na and Mg particles was more favorable than the uptake of MSA on EC and
296 SO_4^{2-} particles. Note that the observations during leg I and leg II were performed under different
297 circumstances, as high concentrations of sea ice were presented during leg I (Fig. S4a) but sea ice
298 free was presented during leg II (Fig. S4b). Despite different conditions were presented during leg
299 I and leg II, the relative fractions of MSA-type particles remained similar, conforming the uptake
300 selectivity of MSA occurred on different particles.

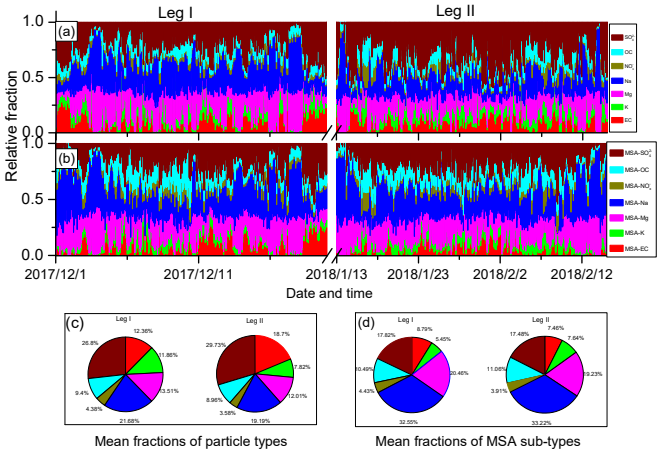

301

https://doi.org/10.5194/acp-2019-811
Preprint. Discussion started: 19 November 2019

Atmospheric Chemistry and Physics Discussions

Fig. 4 Relative fractions of different particle types during leg I and leg II. (a) Relative fractions of different particle types; (b) Relative fractions of MSA-type particles; (c) Average fractions of different particle types during leg I and leg II; and (d) Average fractions of MSA-type particles during leg I and leg II.

The size distributions of total particles and MSA particles are illustrated in Fig. 5. The size of the total particles showed an unimodal distribution, with a mean diameter of 0.51 μm, during leg I and leg II (Fig. 5a). Most of the particles were 0.3-1.0 μm, consisting with particle sizes observed in Antarctica using SMPS (Pant et al., 2011), and with sea spray aerosol sizes measured in marine regions (Quinn et al., 2017). Compare with mean size of the total particles, MSA particles were larger in this study, with a mean diameter of 0.65 μm (Fig. 5a). This suggested that particles were enlarged when MSA uptake occurred on their surfaces. Although particles were enlarged by MSA uptake, submicron MSA particles represented more than 90 % of the total MSA particles (Fig. 5b), indicating that most of the MSA particles were still in the submicron range, consisting with observation results in coastal Antarctica (Legrand et al., 1998) and the Pacific Ocean (Jung et al., 2014).

The size-resolved MSA sub-type particles by population fraction during leg I and leg II were also given in this study. MSA-EC, MSA-K and MSA-NO_x^- particles were primarily distributed in small size (<1 μm) (Fig. 5c). In contrast, high percentage of MSA-Na and MSA-Mg particles were presented in large particles (>1 μm), accounting for more than 75 % of the total coarse particles (Fig. 5c). However, MSA-SO_4^{2-} and MSA-OC particles had a wide size distribution, mainly due to the variety sources for these two types of particles. In this study, SO_4^{2-} was mainly derived from sea salt particles and the oxidation of DMS. Sea salt aerosols generated by whitecaps and bursting bubbles, which were generally in the coarse mode (Norris et al., 2013), while SO_4^{2-} particles generated from the oxidation of DMS were mainly distributed in submicron ranges (Legrand et al., 1998).

https://doi.org/10.5194/acp-2019-811
Preprint. Discussion started: 19 November 2019

Atmospheric Chemistry and Physics Discussions

Although the MSA particle and total particle populations during leg II were much higher than during leg I (Fig. 5a) and seasonal conditions were different between leg I and leg II (Fig. S4), the size-resolved MSA sub-type particles identified during leg II were very similar with the size-resolved MSA sub-type particles identified during leg I (Fig. 5c and 5d), confirming the stable MSA uptake properties on different particles.

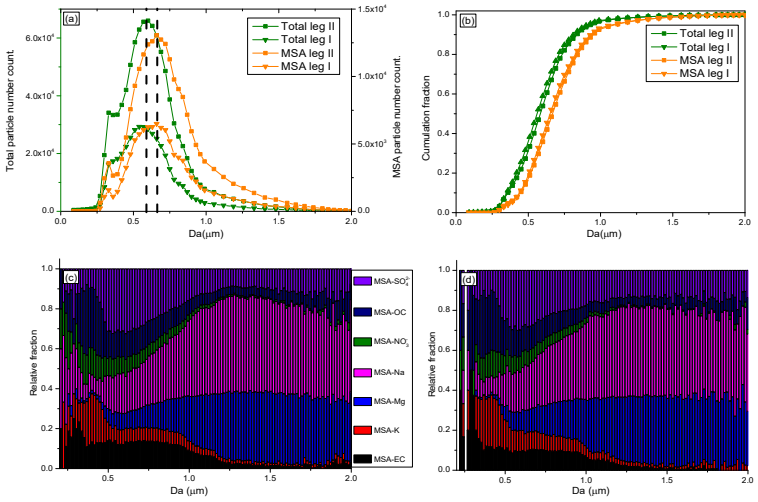

Fig. 5 Size distributions of MSA particles and size-resolved MSA sub-type particles during the cruise, (a) Size distributions of MSA particles and total particles, (b) Cumulative size distributions of MSA and total particles, (c) Size-resolved MSA sub-type particles during leg I, and (d) Size-resolved MSA sub-type particles during leg II.

3.5. The uptake rate of MSA on different particles

The uptake of MSA on the existing particles had been investigated, however, the pressing question was how different aerosol properties impacted the uptake rates of MSA. Fig. 6 shows the uptake rates of MSA (defined as the ratio of MSA-containing particles to the corresponding particles, such as MSA-Na to Na ratio) on different particles in marine atmosphere. The formation of particulate MSA included two routes, the reactive uptake of DMS on existing aerosols, and the conversion of gaseous MSA to particulate MSA through condensation on existing particles (Read et al., 2008). High uptake rates of MSA-Na and MSA-Mg particles were observed in Na and Mg particles, accounting for 0.43 ± 0.21 and 0.41 ± 0.20 of the total Na and Mg particles, respectively (Fig. 6). There were two reasons for the effective uptake of MSA on Na and Mg

https://doi.org/10.5194/acp-2019-811
Preprint. Discussion started: 19 November 2019

Atmospheric Chemistry and Physics Discussions

346 particles. Generally, Na and Mg particles are mainly derived from sea salt particles, which are
347 often alkaline. Previous studies have shown that alkaline sea salt particles were favor to absorb
348 acidic atmospheric gases, promoting the formation of acidic compounds on sea salt particles
349 (Laskin et al., 2003). As an acidic species, MSA was easily absorbed by sea salt particles to form
350 particulate MSA. The other one halogen radicals on the surfaces of sea salt particles also improved
351 the oxidative reactive uptake of DMS on sea salt particles to form particulate MSA (Read et al.,
352 2008).

353 Low uptake rate (0.24 ± 0.68) of MSA-EC particles was observed in this study (Fig. 6). EC
354 particles, emitting from fossil fuel combustion, are highly hydrophobic. In this case, it would
355 suppress the uptake of MSA on EC particles, as DMS reactive uptake often occurred through
356 aqueous reactions (Bardouki et al., 2003). The relative fraction of SO_4^{2-} particles was much higher
357 than that of EC particles (Fig. 4c). However, the uptake rate of MSA-SO_4^{2-} particles (0.26 ±
358 0.47) was similar with that of MSA-EC particles (Fig. 6), indicating that particle population was
359 not the major factor affecting MSA uptake rate. The uptake rate of MSA on existing particles was
360 significant dependent on particle characteristics. As SO_4^{2-} particles were often acidic, MSA uptake
361 by this type of particle was restricted. For this reason, even though the SO_4^{2-} particle population
362 was much higher than Na particle population, the uptake rate of MSA-SO_4^{2-} particles was much
363 lower than that of MSA-Na particles (Fig. 6).

364 Following by the MSA-Na and MSA-Mg particles, the uptake rates of MSA-OC and
365 MSA-NO_x^- particles were 0.37 ± 0.38 and 0.35 ± 0.62, respectively (Fig. 6). This consisted with
366 the relative abundances of MSA-OC and MSA-NO_x^- particles and the corresponding OC and NO_x^-
367 particles (Fig. 4). It indicates that the uptake rates of MSA on existing particles were determined
368 by the aerosol properties, alkaline sea salt particles enhanced the uptake of MSA, while acidic and
369 hydrophobicity species suppressed the uptake of MSA on these particles. The differences of
370 uptake rates of MSA on different types of particles extended the knowledge of DMS oxidation and
371 the formation of particulate MSA in the marine atmosphere.

https://doi.org/10.5194/acp-2019-811
Preprint. Discussion started: 19 November 2019

Atmospheric Chemistry and Physics Discussions

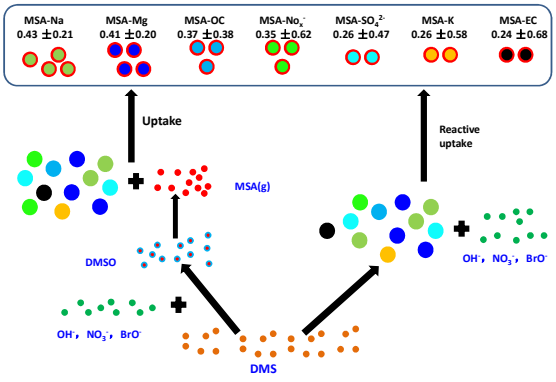

Fig. 6 MSA uptake rates on different aerosol particles in the marine atmosphere.

4. Conclusions

The uptake characteristics of MSA on different aerosols were examined during the early December 2017 and January-February 2018 in the polynya regions of the RS, Antarctica. Particulate MSA mass concentration, as well as particle populations and size distributions, were determined simultaneously for the first time to characterize the formation of MSA on different particles. To access the interactions between MSA and other species, MSA particles were classified into seven sub-types using the ART-2a algorithm: MSA-Na, MSA-Mg, MSA-SO_4^{2-}, MSA-K, MSA-EC, MSA-OC, and MSA-NO_x^-.

MSA mass concentration did not always reflect MSA particle population in the marine atmosphere. MSA uptake occurred on aerosol surfaces altered the aerosol size and chemical compositions, but did not change the aerosol population. MSA particle number count was mainly associated with the total particle number count, as more particles implied a greater opportunity for MSA uptake. High MSA mass concentrations with low MSA population occurred, when low existing particle population with high MSA production from the oxidation of DMS were presented.

The uptake of MSA on existing particles was mainly dependent on aerosol properties. Alkaline sea salt particles enhanced the uptake of MSA, as high uptake rates of MSA-Na and MSA-Mg particles were observed in the Na and Mg particles, accounting for 0.43 ± 0.21 and 0.41 ± 0.20 of

https://doi.org/10.5194/acp-2019-811
Preprint. Discussion started: 19 November 2019

Atmospheric Chemistry and Physics Discussions

the total Na and Mg particles, respectively. But acidic and hydrophobicity species suppressed the uptake of MSA on these particles, as only 0.24 ± 0.68 and 0.26 ± 0.47 of MSA-EC and MSA-SO_4^{2-} were presented in the total EC and SO_4^{2-} particles. The results extend the knowledge of the impact of aerosol properties on the conversion of MSA in the marine atmosphere, however, the details of the formation of MSA are complicated and still controversial. Observations and especially simulation experiments in the laboratory are need in the future to clarify the formation of MSA and their impact factors in the marine atmosphere.

Author contributions

JY conducted the observations, analyzed the results, and wrote the paper. JJ contributed the data analyses and paper writing. MZ conducted the on-board observations. FB and YT contributed to the refining the ideas and contributed considerably to the interpretation of the results. SX and SZ applied the calculations of sea ice distribution and Metrological data. QL and LL contributed the observation data analyses. LC and JY were together responsible for the design of the study. All authors were involved in discussing the results and improved the paper by proofreading.

Acknowledgements

This study is Financially Supported by Qingdao National Laboratory for marine science and technology (No. QNLM2016ORP0109), the Natural Science Foundation of Fujian Province, China (No. 2019J01120), the National Natural Science Foundation of China (No. 21106018, No. 41305133). Jinyoung Jung was supported by grants from Korea Polar Research Institute (KOPRI) (PE19060). The authors gratefully acknowledge Guangzhou Hexin Analytical Instrument Company Limited for the SPAMS data analysis and on-board observation technical assistance, and Zhangjia Instrument Company Limited (Taiwan) for the IGAC technical assistance and data analysis.

References

Adachi, K., Buseck, P. R. Changes in shape and composition of sea-salt particles upon aging in an urban atmosphere. Atmos. Environ. 100, 1-9, 2015.

Allen, J.O. YAADA: Software Toolkit to Analyze Single-Particle Mass Spectral Data, 2005.

Barnes, I., Hjorth, J., Mihalopoulos, N. Dimethyl sulfide and dimethyl sulfoxide and their oxidation in the

https://doi.org/10.5194/acp-2019-811
Preprint. Discussion started: 19 November 2019

Atmospheric Chemistry and Physics Discussions

420 atmosphere. Chem. Rev. 106, 940-975, 2006

421 Bardouki, H., Berresheim, H., Erkoussis, M., Sciare, J., Kouvarakis, G., Oikonomou, K., Schneider, J.,
422 Mihalopoulos, N. Gaseous (DMS, MSA, SO2, H2SO4 and DMSO) and particulate (sulphate and
423 methanesulfonate) sulphur species over the northeastern coast Crete. Atmos. Chem. Phys. 3, 1871-1886,
424 2003.

425 Bates, T. S., Calhoum, J. A., Quinn, P. K. Variations in the methane sulphonate to sulphate molar ratio in
426 submicrometer marine aerosol particles over the South Pacific Ocean. J. Geophys. Res. 97, 9859-9865, 1992.

427 Bork, N., Elm, J., Olenius, T., Vehkamaki. Methane sulfonic acid-enhanced formation of molecular clusters of
428 sulfuric acid and dimethyl amine. Atmos. Chem. Phy. 14, 12023-12030, 2014.

429 Casillas-Ituarte, N.N., Callahan, K. M., Tang, C.Y., Chen, X., Roeselova, M. Surface organization of aqueous
430 MgCl2 and application to atmospheric marine aerosol chemistry. PNAS, 107, 6616-6621, 2010.

431 Cavalieri, D. J., and Parkinson, C. L. 30-Year satellite record reveals contrasting Arctic and Antarctic decadal sea
432 ice variability. Geophys. Res. Lett. 30(18), 2003.

433 Chang, R. Y.-W., Sjostedt, S. J., Pierce, J. R., Papakyriakou, T. N., Scarratt, M. G., Michaud, S., et al. Relating
434 atmospheric and oceanic DMS levels to particle nucleation events in the Canadian Arctic. J. Geophys. Res.
435 116, D00S03, 2011.

436 Chen, L., Wang, J., Gao, Y., Xu, G., Yang, X., Lin, Q., Zhang, Y. Latitudinal distributions of atmospheric MSA and
437 MSA/nss-SO42- ratios in summer over the high latitude regions of the Southern and Northern Hemispheres. J.
438 Geophys. Res. 117, D10306, 2012.

439 Davis, D., Chen, G., Kasibhatla, P., Jefferson, A., Tanner, D., Eisele, F., Lenschow, D., Neff, W., Berresheim, H.
440 DMS oxidation in the Antarctic marine boundary layer: Comparison of model simulations and field
441 observations of DMS, DMSO, $DMSO_2$, $H_2SO_4(_g)$, $MSA(_g)$, and $MSA(_p)$. J. Geophys. Res. 103, 1657-1678,

https://doi.org/10.5194/acp-2019-811
Preprint. Discussion started: 19 November 2019

Atmospheric Chemistry and Physics Discussions

1998.

De Baar, H. J., De Jong, J. T., Bakker, D. C., Löscher, B. M., Veth, C., Bathmann, U., Smetacek, V. Importance of iron for plankton blooms and carbon dioxide drawdown in the Southern Ocean. Nature, 373, 412-415, 1995.

Gaston, C.J., Furutani, H., Guazzotti, S. A., Coffee, K.R., Bates, T.S., Quinn, P.K., Aluwihare, L.I. Mitchell, B.G., Prather, K. Unique ocean-derived particles serve as a proxy for changed in ocean chemistry. Journal of Geophysical Research, 116, D18310, 2011

Guazzotti, S. A., Coffee, K. R., Prather K. A. Continuous measurements of size‐resolved particle chemistry during INDOEX Intensive Field Phase 99, J. Geophys. Res., 106(D22), 28,607 – 28,627, doi:10.1029/2001JD900099, 2001.

Ghahremaninezhad, R., Norman, A.-L., Abbatt, J. P. D., Levasseur, M., Thomas, J. L. Biogenic, anthropogenic and sea salt sulfate size-segregated aerosols in the Arctic summer. Atmos. Chem. Phy. 16, 5191-5202, 2016.

Hayashida, H., Steiner, N., Monahan, A., Galindo, V., Lizotte, M., Levasseur, M. Implications of sea-ice biogeochemistry for oceanic production and emissions of dimethyl sulfide in the Arctic. Biogeosciences. 14, 3129-3155, 2017.

Healy, R. M., Hellebust, S., Kourtchev, I., Allanic, A., O'Connor, I. P., Bell, J. M., Healy, D. A., Sodeau, J. R., Wenger, J. C. Source apportionment of $PM_{2.5}$ in Cork Harbour, Ireland using a combination of single particle mass spectrometry and quantitative semi-continuous measurements. Atmos. Chem. Phy. 10, 9593-9613, 2010.

Horne, J.R., Zhu, S., Montoya-Aguilera, J., Hinks, M.L., Wingen, L.M., Nizkorodov, S.A., Dabdub,D. Reactive uptake of ammonia by secondary organic aerosols: Implications for air quality. Atmos. Environ. 189, 1-8, 2018.

Jung, J., Furutani, H., Uematsu, M., Park, J.. Distributions of atmospheric non-sea-salt sulfate and methanesulfonic acid over the Pacific Ocean between 48°N and 55°S during summer. Atmos. Environ. 99, 374-384, 2014.

https://doi.org/10.5194/acp-2019-811
Preprint. Discussion started: 19 November 2019

Atmospheric Chemistry and Physics Discussions

464 Kloster, S., Feichter, J., Maier-Reimer, E., Six, K. D., Stier, P., Wetzel, P. DMS cycle in the marine
465 ocean-atmosphere system? a global model study. Biogeosciences, 3, 29-51, 2006.
466 Laskin, A., Gaspar, D.J., Wang, W., Hunt, S. W., Cowin, J.P., Colson, S.D., Finlayson-Pitts, B.J. Reactions at
467 interfaces as a source of sulfate formation in sea-salt particles. Science, 301(5631), 340-344, 2003.
468 Legrand, M., Pasteur, E. C. Methane sulfonic acid to non-sea-salt sulfate ratio in coastal Antarctic aerosol and
469 surface snow. J. Geophys. Res. 103, 10991-11006, 1998.
470 Li, L., Huang, Z., Dong, J., Li, M., Gao, W., Nian, H., Fu, Z., Zhang, G., Bi, X., Cheng, P., Zhou, Z. Real time
471 bipolar time-of-flight mass spectrometer for analyzing single aerosol particles. Int. J. Mass Spectrom. 303,
472 118-124, 2011.
473 Li, L., Li, M., Huang, Z.X., Gao, W., Nian, H.Q., Fu, Z., Gao, J., Chai, F.H., Zhou, Z. Ambient particle
474 characterization by single particle aerosol mass spectrometry in an urban area of Beijing. Atmos. Environ. 94,
475 323-331, 2014.
476 Liu, M., Song, Y., Zhou, T., Xu, Z., Yan, C., Zheng, M., Wu, Z., Hu, M., Wu, Y., Zhu, T. Fine particle pH during
477 severe haze episodes in northern China, Geophys. Res. Lett. 44, 5213-5221, 2017.
478 Lizotte, M. P. The Contributions of Sea Ice Algae to Antarctic Marine Primary Production. Am. Zool. 41, 57-73,
479 2001.
480 Loose, B., Miller, L. A., Elliott, S., Papakyriakou, T. Sea ice biogeochemistry and material transport across the
481 frozen interface. Oceanography, 24, 202-218, 2011.
482 Minikin, A., Legrand, M., Hall, J., Wagenbach, D., Kleefeld, C., Wolff, E., Pasteur, E. C., Ducroz, F.
483 Sulfur-containing species (sulfate and methanesulfonate) in coastal Antarctic aerosol and precipitation, J.
484 Geophys. Res., 103, 10975-10990, 1998.
485 Murphy, S. M., Agrawal, H., Sorooshian, A., Padró, L.T., Gates, H., Hersey, S. Comprehensive simultaneous

https://doi.org/10.5194/acp-2019-811
Preprint. Discussion started: 19 November 2019

Atmospheric Chemistry and Physics Discussions

shipboard and airborne characterization of exhaust from a modern container ship at sea. Environ. Sci. Tech. 43, 4626-4640, 2009.

Norris, S. J., Brooks, I. M., Moat, B. I., Yelland, M. J. Near-surface measurement of sea spray aerosol production over whitecaps in the open ocean. Ocean Sci. 9, 133-145, 2013.

Pant, V., Siingh, D., Kamra, A.K., Size distribution of atmospheric aerosols at Maitri, Antarctica. Atmospheric Environment, 45, 5138-5149, 2011.

Preunkert, S., Jourdain, B., Legrand, M., Udisti, R., Becagli, S., Cerri, O. Seasonality of sulfur species (dimethyl sulfide, sulfate, and methanesulfonate) in Antarctica: Inland versus coastal regions. J. Geophys. Res. 113, D15302, 2008.

Preunkert, S., Legrand, M., Jourdain, B., Moulin, C., Belviso, S., Kasamatsu, N., Fukuchi, M., Hirawake, T. Interannual variability of dimethylsulfide in air and seawater and its atmospheric oxidation by-products (methanesulfonate and sulphate) at Dumont d'Urville, coastal Antarctica (1999-2003). J. Geophys. Res. 112, 2007.

Quinn, P.K., Coffman, D.J., Johnson, J.E., Upchurch, L.M., Bates, T.S. Small fraction of marine cloud condensation nuclei made up of sea spray aerosol, Nature Geoscience, doi:10.1038/NGEO3003, 2017.

Quinn, P.K., Bates, T.S., Schulz, K.S., Coffman, D.J., Frossard, A.A., Russell, L.M., Keene, W.C., Kieber, D.J. Contribution of sea surface carbon pool to organic matter enrichment in sea spry aerosol. Nature Geos. 7, 228-232, 2014.

Read, K. A., Lewis, A. C., Bauguitte, S., Rankin, A. M., Salmon, R. A., Wolff, E. W., Saiz-Lopez, A., Bloss W. J., Heard, D. E., Lee, J. D., Plane, J. M. C. DMS and MSA measurements in the Antarctic Boundary Layer: impact of BrO on MSA production. Atmos. Chem. Phys. 8, 2985-2997, 2008.

Savoie, D.L., Prospero, J.M., Larsen,R.J., Huang, F., Izaguirre, M.A., Huang, T., Snowdon, T.H., Custals, L.,

https://doi.org/10.5194/acp-2019-811
Preprint. Discussion started: 19 November 2019

Atmospheric Chemistry and Physics Discussions

508 Sanderson, C.G. Nitrogen and sulfur species in Antarctic aerosols at Mawson, Palmer, and Marsh (King
509 George Island), J. Atmos. Chem. 17, 95-122, 1993.

510 Song, X.H., Hopke, P.K., Fergenson, D.P., Prather, K.A. Classification of single particles analyzed by ATOFMS
511 using an artificial neural network, ART-2A. Analy. Chem. 71, 860-865, 1999.

512 Sorooshian, A., Lu, M. L., Brechtel, F. J., Jonsson, H., Feingold, G., Flagan, R.C., Seinfeld, J.H. On the source of
513 organic acid aerosol layers above clouds. Environ. Sci. Technol. 41, 4647-4654, 2007.

514 Spreen, G., Kaleschke, L., and Heygster, G. Sea ice remote sensing using AMSR-E 89 GHz channels, J. Geophys.
515 Res., 113, C02S03, 2008.

516 Silva, P. J., Carlin, R. A., Prather, K. A. Single particles analysis of suspended soil dust from Southern California.
517 Atmos. Environ. 34, 1811-1820, 2000.

518 Sitaras, I. E., Siskos, P. A. The role of primary and secondary air pollutants in atmospheric pollution: Athens urban
519 area as a case study. Environ. Chem. Lett. 6, 59-69, 2008.

520 Tao, J., Zhang, Z., Tan, H., Zhang, L., Wud, Y., Sun, J., Chee, H., Cao, J., Cheng, P., Chen, L., Zhang, R.
521 Observation evidence of cloud processes contributing to daytime elevated nitrate in an urban atmosphere.
522 Atmos. Environ. 186, 209-215, 2018.

523 Taylor, M. H., Losch, M., Bracher, A. On the drivers of phytoplankton blooms in the Antarctic marginal ice zone:
524 A modeling approach. J. Geophys. Res. 118, 63-75, 2013.

525 Teinila, K., Frey, A., Hillamo, R., Tulp, H. C., Weller, R. A study of the sea-salt chemistry using size-segregated
526 aerosol measurements at coastal Antarctic station Neumayer. Atmos. Environ. 96, 11-19, 2014.

527 Tian, M., Wang, H., Chen, Y., Zhang, L., Shi, G., Liu, Y., Yu, J., Zhai, C., Wang, J., Yang, F. Highly time-resolved
528 characterization of water-soluble inorganic ions in PM2.5 in a humid and acidic mega city in Sichuan Basin,
529 China. Sci. Total Environ. 580, 224-234, 2017.

https://doi.org/10.5194/acp-2019-811
Preprint. Discussion started: 19 November 2019

Atmospheric Chemistry and Physics Discussions

530 Wang, S., Bailey, D., Lindsay, K., Moore, J. K., Holland, M. Impact of sea ice on the marine iron cycle and
531 phytoplankton productivity. Biogeosciences, 11, 4713-4731, 2014.
532 Weller, R., Legrand, M., Preunkert, S. Size distribution and ionic composition of marine summer aerosol at the
533 continental Antarctic site Kohnen. Atmos. Chem. Phys., 18, 2413-2430, 2018.
534 Yan, J., Lin, Q., Zhao, S., Chen, L., Li, L. Impact of marine and continental sources on aerosol characteristics
535 using an on-board SPAMS over Southeast Sea, China. Environ. Sci. Pollution Res. 25, 30659-30670, 2018.
536 Young, L. H., Li, C. H., Lin, M. Y., Hwang, B. F., Hsu, H. T., Chen, Y. C., Jung, C. R., Chen, K. C., Cheng, D. H.,
537 Wang, V. S., Chiang, H. C., Tsai, P. J. Field performance of semi-continuous monitor for ambient PM2.5
538 water-soluble inorganic ions and gases at a suburban site. Atmos. Environ. 144,376-388, 2016.
539 Zhang, M., Chen, L., Xu, G., Lin, Q., Liang, M. Linking phytoplankton activity in polynyas and sulfur aerosols
540 over Zhongshan Station, East Antarctica. J. Atmos. Sci. 72, 4629-4642, 2015.